BioOne COMPLETE

The Surface Energy Budget in the Accumulation Zone of the Laohugou Glacier No. 12 in the Western Qilian Mountains, China, in Summer 2009

Authors: Sun, Weijun, Qin, Xiang, Ren, Jiawen, Yang, Xingguo, Zhang, Tong, et al.

The Surface Energy Budget in the Accumulation Zone of the Laohugou Glacier No. 12 in the Western Qilian Mountains, China, in Summer 2009

Weijun Sun‡*

*Xiang Qin**

*Jiawen Ren**

Xingguo Yang†

*Tong Zhang**

*Yushuo Liu**

Xiaoqing Cui and*

*Wentao Du**

*State Key Laboratory of Cryospheric Sciences/Qilian Shan Station of Glaciology and Ecologic Environment, Cold and Arid Regions Environmental and Engineering Research Institute, Chinese Academy of Sciences, Lanzhou 730000, China

†Key Laboratory of Arid Climatic Change and Reducing Disaster, Institute of Arid Meteorology, CMA, Lanzhou 730020, China

‡Corresponding author: sun1982wj@163.com

Abstract

The energy balance of a glacial surface can describe physical melting processes. To expand the understanding of how glaciers in arid regions respond to climate change, the energy budget in the accumulation zone of the Laohugou Glacier No. 12 was measured. Input variables were meteorological data (1 June–30 September 2009) from an automatic weather station located on the accumulation zone at 5040 m above sea level (a.s.l.). Radiative fluxes directly measured, and turbulent fluxes calculated using the bulk aerodynamic approach, were involved in the surface energy budget. Net radiation flux was the primary source of the surface energy balance (72%) and was chiefly responsible for glacial melting, followed by sensible heat flux (28%). Melting energy was the main output of surface energy (48%), and was almost as large as the sum of latent heat flux (32%) and subsurface heat flux (20%). The modeled mass balance was -75 mm water equivalent, which compared well with sonic ranging sensor readings. Albedo varied between 0.52 and 0.88 on the glacial surface, and melting was prevented by high albedo. Under the assumption of neutral atmospheric conditions, turbulent fluxes were overestimated, especially the sensible heat flux by 54%; therefore, a stability correction was necessary.

Introduction

Glacier melting, which impacts on the dynamic change of glaciers over a range of spatial and temporal scales, has a close relationship with energy exchange between the atmosphere and the glacial surface. The physical melting process at the glacial surface can be described by the energy balance melt model. Therefore, it is important to investigate the hydrothermal conditions of glacial evolution, and the relationship between climate and glaciers (Shi, 1988). The study of glacial surface energy balance has been carried out in Greenland (e.g., Oerlemans, 1991; Van As, 2011), Antarctica (e.g., Van den Broeke et al., 2004a; Hoffman et al., 2008), and on glaciers in other mountainous regions of the world (e.g., Greuell and Smeets, 2001; Wagnon et al., 2003; Mölg and Hardy, 2004; Klok et al., 2005). In China, surface energy balance experiments have been conducted in the Tianshan Mountains (e.g., Kang and Ohmura, 1994; Li et al., 2007), the Tanggula Mountains (e.g., Zhang et al., 1996), and the Qilian Mountains (e.g., Chen et al., 2007; Jiang, 2008), but these studies have focused on the ablation zone of glaciers. Little is known about the surface energy balance in the accumulation zone of glaciers in the Qinghai-Tibet Plateau, especially in arid regions. To improve understanding of the relationship between different climate forcing and glacial ablation in the accumulation zone of glaciers, an automatic weather station (AWS) was installed at 5040m a.s.l. on the Laohugou Glacier No. 12 in the western Qilian Mountains. This AWS obtains continuous measurements of the energy exchange between the atmosphere and the glacial surface.

In this study we aim to quantify the component proportion of the energy fluxes at the glacier surface in the accumulation zone using meteorological observation. We discuss the effect of albedo, precipitation, and daily positive accumulated temperature on the glacier melting, and evaluate the sensitivity of the sensible and latent heat fluxes to uncertainty in parameter values and meteorological variables. Our results enable us to identify the characteristics of the surface energy budget in the accumulation zone of the Laohugou Glacier No. 12, located in a cold, high altitude, arid region.

Location and Measurement Program

The Laohugou Glacier No. 12 is located in the north of the western Qilian Mountains at 39°26.4′N, 96°32.5′E (Fig. 1). The glacier consists of two tributaries, is 9.85 km long, has a total area of 20.4 km² (Du et al., 2008), and extends from 5481m a.s.l. to 4260 m a.s.l. (Liu et al., 2010). The accumulation zone is both wide (1.5 km), and flat (3–6° of slope angle) (Wang, 1981), and is therefore suitable for installation of an AWS for meteorological observation. The physical characteristics of the glacier make it the most typical continental glacier in the Laohugou Valley.

The AWS was set up on a relatively flat surface in the accumulation zone of the Laohugou No. 12 Glacier (39°25.7′N, 96°33.4′E, 5040 m a.s.l.; Fig. 1), and started operating on 23 May 2009. The
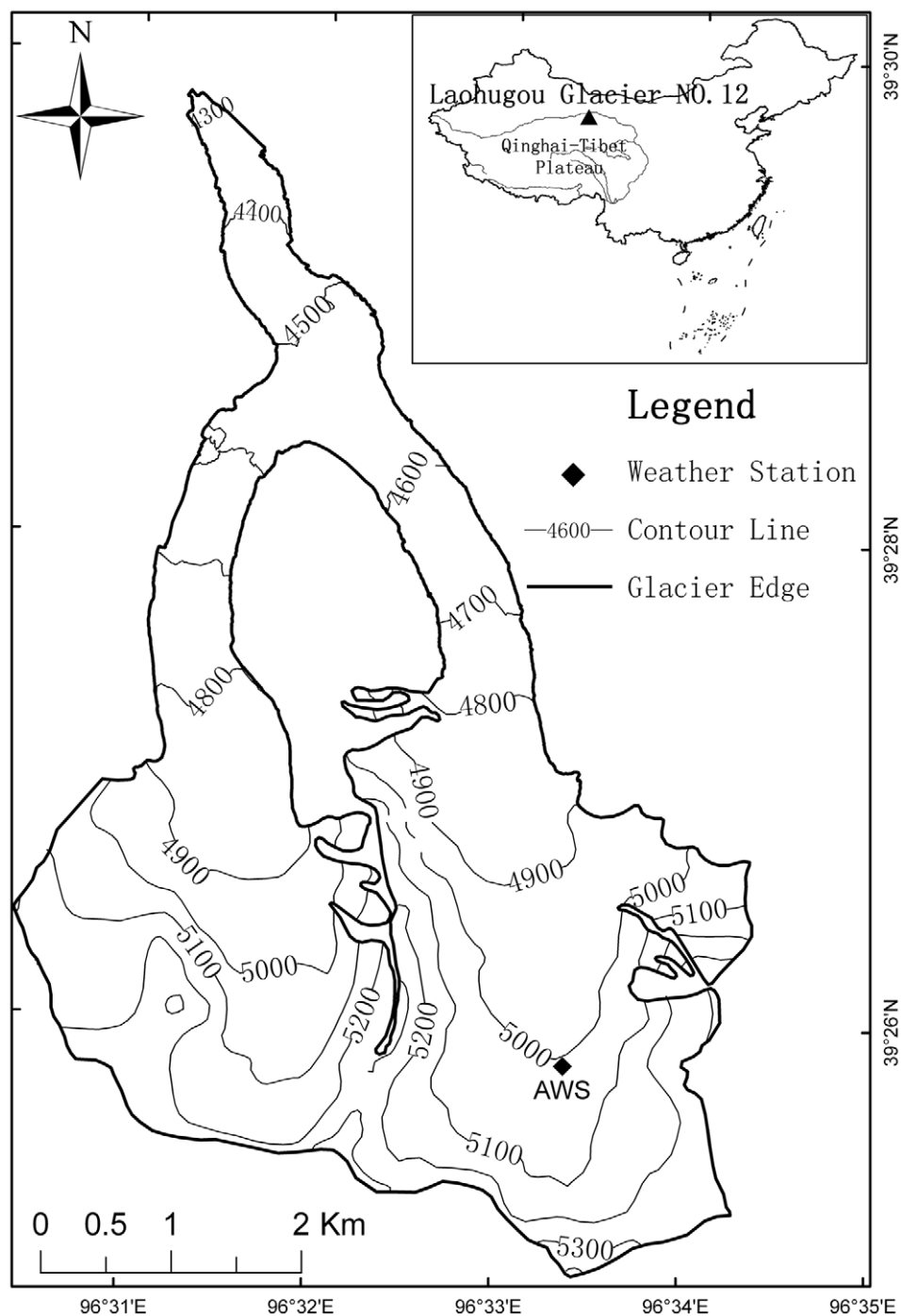
FIGURE 1. The Laohugou Glacier No. 12 in the Qilian Mountains, China. Contours are in meters.

station was visited, and sensors were checked, every 14–21 days during the field investigation period (from May to October 2009). The data collected by the AWS included air pressure, incident and reflected shortwave radiation ($S\downarrow$ and $S\uparrow$), incoming and outgoing long-wave radiation ($L\downarrow$ and $L\uparrow$), 2-level air temperature and humidity, and wind speed and direction (Table 1). Solid precipitation was measured in mm w.e. (mm water equivalent) using a Geonor T-200B gauge, an accumulative weighing bucket precipitation gauge without heating. All sensors were connected to a data logger (CR1000, Campbell, U.S.A.) with a low temperature resistance (-55 °C), and the AWS recorded the half-hourly mean of the measurements taken every 10 s. The meteorological data were collected from 1 June to 30 September 2009. The local time at the AWS was 1 h 34 min later than Beijing Time, and Beijing Time (BJT) was used throughout this study.

Data Processing

Snow cover and rime formation upon the dome of the radiation sensors and low sun angle are the main factors affecting the measurement of radiation (Van den Broeke et al., 2004a). The upward-facing side of the sensor is more sensitive to icing than

WEIJUN SUN ET AL. / 297

TABLE 1

The automatic weather station: technical parameters and installation heights of sensors.

Element	Sensor Type	Accuracy According to the Manufacturer	Height
Air temperature, °C	Vaisala41382	±0.2 °C	1.5 m, 3.5 m
Relative humidity, %	Vaisala41382	±2%	1.5 m, 3.5 m
Air pressure, hPa	PTB210	±0.5 hPa	1.5 m
Wind speed, m s^{-1}	Young05103	±0.3 m s^{-1}	1.5 m, 3.5 m
Wind direction, °	Young05103	±3°	1.5 m, 3.5 m
Shortwave radiation, W m^{-2}	CNR1	±10% for daily total	1.5 m
Longwave radiation, W m^{-2}	CNR1	±10% for daily total	1.5 m
Snow depth, cm	Campbell SR50	±1 cm	2.0 m
Precipitation, mm w.e.	Geonor T200B	±0.1%	1.7 m

the underside. Snow cover will generally lead to an underestimation of $S\downarrow$, and $S\downarrow$ can be overestimated when the sun angle is low, because the thin ice coating can diffract the sun's rays onto the sensor plate (Van den Broeke et al., 2004b). Since the study site has a dry climate with high winds, the above factors have little impact on $S\uparrow$ and $L\uparrow$. Normally the sun's rays have a large tilt angle in the early morning and late afternoon, and as a result $S\downarrow$ becomes smaller than $S\uparrow$, and the albedo is higher than 0.9. To compute the net shortwave radiation (S_{net}) accurately, the "accumulated albedo" can be used (Van den Broeke et al., 2004b):

$$S_{net} = -S\uparrow(1+\alpha)/\alpha \qquad (1)$$

$$\cong -S\uparrow(1+\alpha_{acc})/\alpha_{acc}$$

$$\alpha_{acc} = \frac{\sum_{24h} S\uparrow}{\sum_{24h} S\downarrow} \qquad (2)$$

where α_{acc} is an "accumulated" albedo, that is, the ratio of accumulated $S\uparrow$ and $S\downarrow$ over a time window of 24 h centered on the observation time.

The underlying glacial surface is covered with snow all the year round, and the energy balance at the snow surface is expressed as follows (fluxes are in W m^{-2}, and considered positive when directed toward the surface):

$$R_n + H + LE + P + Q_G = Q_M \qquad (3)$$

where R_n is the net radiation, H is the sensible heat flux, and LE is the latent heat flux. The heat advected by precipitation P is small and negligible compared to other fluxes. Q_G symbolizes the total energy flux in the subsurface. Q_M is the energy used for melting (positive) or freezing (negative). The surface energy balance is calculated at half-hourly intervals.

Based on the Monin-Obukhov similarity theory, the bulk aerodynamic approach, including stability correction, is used to calculate turbulent heat fluxes. This method can yield the best correlation to the eddy-covariance measurements, particularly when air temperature is below freezing (Arck and Scherer, 2002). The analytical expressions for turbulent fluxes are as follows (e.g., Oke, 1987):

$$H = \rho \frac{C_P k^2 u(T - T_S)}{\ln(\frac{z}{z_{om}})\ln(\frac{z}{z_{ot}})}(\Phi_m\Phi_h)^{-1} \qquad (4)$$

$$LE = \rho \frac{L_S k^2 u(q - q_S)}{\ln(\frac{z}{z_{om}})\ln(\frac{z}{z_{oq}})}(\Phi_m\Phi_v)^{-1} \qquad (5)$$

where $\rho = (\rho_o P)/P_o$ is the air density at 5040 m a.s.l., ρ_o and P_o are the air density (1.29 kg m^{-3}) and the air pressure (1013 hPa), respectively, at standard sea level, and P is the air pressure at the measurement site (hPa). C_P is the specific heat capacity for air at constant pressure [$C_P = C_{pd}(1 + 0.84q)$ with $C_{pd} = 1005$ J kg^{-1} K^{-1}, the specific heat capacity for dry air at constant pressure], and k is the von Karman constant ($k = 0.4$). T, u, and q are mean values of air temperature (K), wind speed (m s^{-1}), and specific humidity, respectively, at the height of z, and q_S is the surface specific humidity calculated using glacial surface saturation vapor pressure e_s, $q_S \approx \epsilon e_s/P$ ($\epsilon = 0.622$); e_s can be computed using T_S, $e_s = 6.112\exp[17.67T_S/(T_S + 243.5)]$ (Bolton, 1980). T_S is the surface temperature (K), which is derived from $L\uparrow$ using the Stefan-Boltzmann equation assuming that the emissivity of the snow is unity, $L\uparrow = \sigma T_S^4$ with $\sigma = 5.67\ 10^{-8}$ W m^{-2} K^{-4} (e.g., Brugman, 1991). L_S is the latent heat of sublimation of snow or ice (2.834 MJ Kg^{-1}), and z_{om}, z_{ot}, and z_{oq} are the surface roughness lengths (m) for momentum, temperature, and humidity, respectively. The nondimensional stability functions for momentum (Φ_m), heat (Φ_h), and moisture (Φ_v), may be expressed in terms of Ri_b (bulk Richardson number), which relates the relative effects of buoyancy to mechanical forces (e.g., Oke, 1987):

for Ri_b positive (stable): $(\Phi_m\Phi_h)^{-1} = (\Phi_m\Phi_v)^{-1}$ (6)
$$= (1 - 5Ri_b)^2$$

for Ri_b negative (unstable): $(\Phi_m\Phi_h)^{-1} = (\Phi_m\Phi_v)^{-1}$ (7)
$$= (1 - 16Ri_b)^{0.75}$$

where Ri_b is used to describe the stability of the surface layer, and can be expressed as:

$$Ri_b = \frac{g\frac{(T-T_S)}{(z-z_{om})}}{T(\frac{u}{z-z_{om}})^2} = \frac{g(T-T_s)(z-z_{om})}{Tu^2} \qquad (8)$$

where g is the acceleration of gravity (9.8 m s^{-2}). When wind speed is low (<1 m s^{-1}), it can lead to unrealistically high values for Ri_b (>1), and turbulence will disappear if the vertical temperature stratification becomes very stable (Roode et al., 2010).

Snow crystals transform slowly when temperature is low, and as a result snow surface roughness elements in the accumulation

zone only vary slightly. Therefore, a constant, z_{om}, can be used for the entire experiment. $z_{om}(9 \times 10^{-4}$ m) was determined from the calculation of the wind velocity profile law at ''near-neutral'' conditions (e.g., Greuell and Smeets, 2001; Denby and Snellen, 2002), using measurements at 1.5 and 3.5 m levels. The half-hourly average profiles were used to calculate z_{om} if the following criteria were met: (1) u at 3.5 m > u at 1.5 m; (2) u at 1.5 m > 3.5 m s^{-1}, to ensure well mixed turbulence flow conditions; (3) near-neutral conditions, defined by $-0.02 \leq Ri_b \leq 0.02$. According to Andreas (1987), z_{ot} (2.4 $\times10^{-4}$ m) and z_{oq} (3.0 $\times10^{-4}$ m) could be obtained from z_{om} and the roughness Reynolds number.

Q_G comprises a heat flux from penetrating shortwave radiation (Q_S) and a conductive energy flux (Q_C). The former is calculated as a 10% fraction of S_{net} for days with snow at the glacial surface (Bintanja and Van den Broeke, 1995). The latter is estimated from the temperature-depth profile and can be given by: $Q_C = -k_T(\partial T'/\partial_{z'})$, where k_T is the thermal conductivity, 0.4 W m^{-1} K^{-1} for old snow, and 2.2 W m^{-1} K^{-1} for pure ice (Oke, 1987). Q_C was computed from T_S and an observed temperature of -3.9 °C at a depth of 14 m, which was relatively stable from 1 June to 30 September.

For half-hourly steps, sublimation M_S is calculated from negative latent heat flux, $M_S = LE/L_S$. When T_S, found using the Stefan-Boltzmann equation, exceeds the melting point, T_S is set back to 0 °C and the surface melt M is computed from the melting energy, $M = Q_M/L_f$, with L_f as the heat constant for fusion (0.334 MJ kg^{-1}).

Climate Conditions

The Laohugou Valley is characterized by the typical continental climate under the influence of the westerlies all year-round. At 4200 m a.s.l., daily mean temperature in summer (from 1 June to 30 September) is above 0 °C, and precipitation occurs mainly from May to September. Daily means of air and glacial surface temperatures, specific humidity of air and glacial surface, and wind speed in the accumulation zone at 5040 m a.s.l. from 1 June to 30 September 2009 are shown in Figure 2. The standard deviation was 0.6

°C for air temperature and 0.07 g kg^{-1} for specific humidity. Compared to air temperature and specific humidity, variations of glacial surface temperature and specific humidity were larger, but fluctuations were not pronounced. Average air and glacial surface temperatures were -2.6 °C and -6.4 °C, respectively, and the difference between them influenced the sensible heat flux between the atmosphere and glacial surface. In addition, there were 90 days when air temperature reached higher than 0 °C. Mean air and glacial surface specific humidity were 3.7 g kg^{-1} and 4.6 g kg^{-1}, respectively, and latent heat flux was affected by their difference. Precipitation, which has an effect on the accumulation and ablation of the glacier, was 317 mm w.e. during the observation period (see later in Fig. 8). Precipitation occurred on 58 days, and the maximum monthly precipitation (142 mm w.e.) appeared in July, and accounted for 36% of the annual precipitation. Wind speed, which played a significant role in the turbulent exchange between the atmosphere and the glacial surface, had a daily mean of 2.8 m s^{-1}.

Results

RADIATION FLUXES AND ALBEDO

$S\downarrow$ is impacted by strong convective weather, good atmospheric transparency, and reflection influenced by surrounding mountains (Yang et al., 2010). There is an abundant solar energy resource at the measurement site, and the monthly mean of $S\downarrow$ in June, 332 W m^{-2}, was larger than the maximum for the Tanggula region, 249 W m^{-2} (Yao, 2009), because there were more sunny days in the Laohugou Valley. Figure 3 illustrates the characteristics of the components of radiation. $S\downarrow$ was unstable during the observation period, varying between 138 and 412 W m^{-2}. The fluctuation of $S\uparrow$ was similar to that of $S\downarrow$, varying between 112 and 313 W m^{-2}. $L\uparrow$ was relatively stable, while $L\downarrow$ varied widely because of the effect of the cloud cover. Therefore, the variation of L_{net} was mainly governed by $L\downarrow$. The mean values of $L\downarrow$ and $L\uparrow$ were 234 and 288 W m^{-2}, respectively. The mean value of $L\uparrow$ was as large as the value measured on the Rongbuk Glacier on the north slope of Mt. Everest, 289 W m^{-2} (Yang et al., 2010), because both
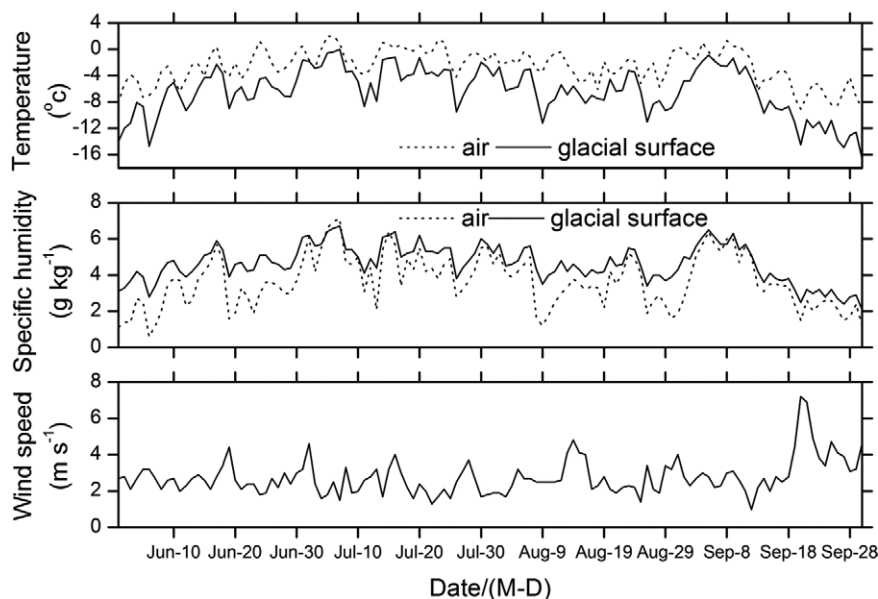

FIGURE 2. Daily mean values of air temperature (1.5 m), glacial surface temperature, air specific humidity (1.5 m), glacial surface specific humidity, and wind speed (1.5 m) on the Laohugou Glacier No. 12 in the Qilian Mountains from 1 June to 30 September 2009.
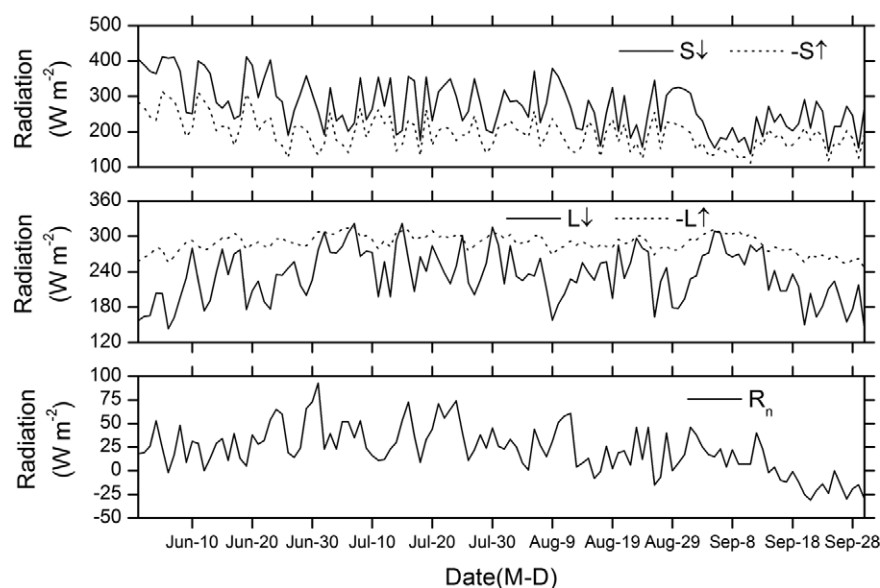
FIGURE 3. Daily mean values of incident ($S\downarrow$) and reflected ($S\uparrow$) shortwave radiation, incoming ($L\downarrow$) and outgoing ($L\uparrow$) longwave radiation, and net radiation (R_n) on the Laohugou Glacier No. 12 in the Qilian Mountains from 1 June to 30 September 2009.

stations were in the accumulation zone and covered with snow. However, the mean value of $L\uparrow$ was less than that for the McCall Glacier in the Romanzof Mountains (Klok et al., 2005), because the AWS on the McCall Glacier was located in ablation zone with an ice surface. R_n remained positive throughout most of the observation period, until September 15, when it became negative with variations between -31 and 93 W m^{-2}. With the influence of precipitation and high daily positive accumulated air temperature, the curve of albedo showed large fluctuation. Values varied between 0.52 and 0.88 during the observation period (see later in Fig. 8), with sustained high values at the beginning of June and the end of September. Albedo had an effect on the variation of R_n, with a negative relationship ($r = -0.54$, $n = 122$).

Mean diurnal cycles of the radiative terms during the observation period are presented in Figure 4. During the daytime, $S\uparrow$ followed the diurnal variations of $S\downarrow$, and both reached maximum

levels at 12:30 BJT after the station received the first sun rays at 06:30 BJT. $S\downarrow$ decreased with the decreasing angle of the sun until sunset. R_n followed the diurnal variation of $S\downarrow$ but became positive with a delay. $L\downarrow$ and $L\uparrow$ reached maximum levels at 14:00 BJT, a consequence of the maximum air temperature occurring at the time (see later in Fig. 6).

SENSIBLE AND LATENT HEAT FLUXES

Figure 5 illustrates the daily mean variations of H, LE, and the sum of $H + LE$. H was positive most of the time, and LE was negative throughout most of the observation period, but became positive on some days, implying that condensation had occurred. Daily mean values of H varied between -2.9 and 66 W m^{-2}, and were negative on 5 and 15 June, 3 July, and 2 August, with precipitation occurring, indicating that heat transferred from the
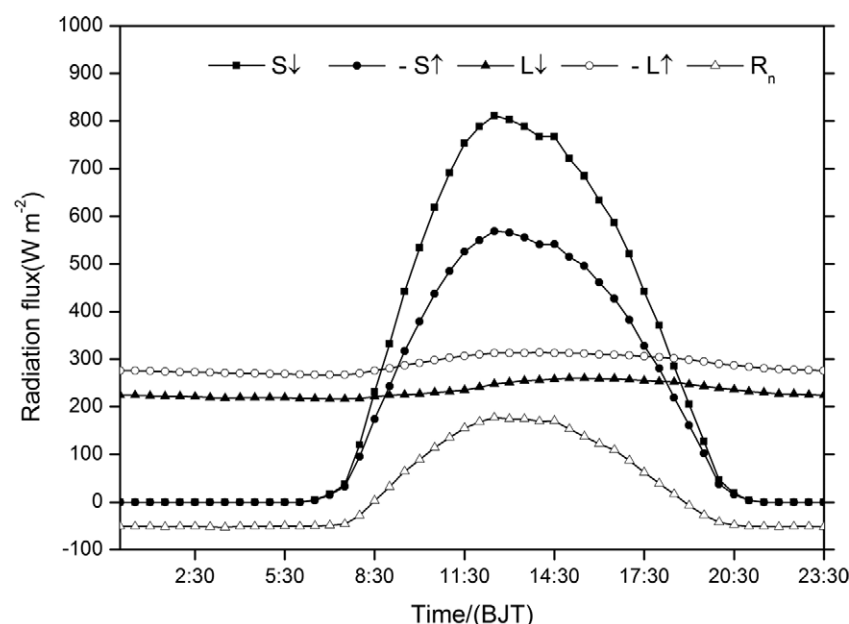

FIGURE 4. Mean diurnal cycles of incident ($S\downarrow$) and reflected ($S\uparrow$) shortwave radiation, incoming ($L\downarrow$) and outgoing ($L\uparrow$) longwave radiation, and net radiation (R_n) on the Laohugou Glacier No. 12 in the Qilian Mountains from 1 June to 30 September 2009.
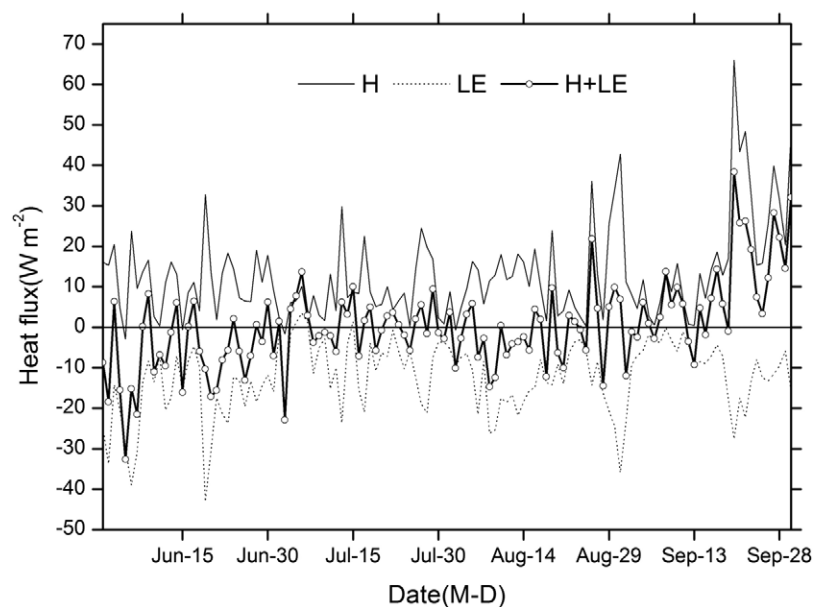
300 / Arctic, Antarctic, and Alpine Research

FIGURE 5. Daily mean values of sensible (*H*) and latent (*LE*) heat fluxes and the sum (*H* + *LE*) on the Laohugou Glacier No. 12 in the Qilian Mountains from 1 June to 30 September 2009.
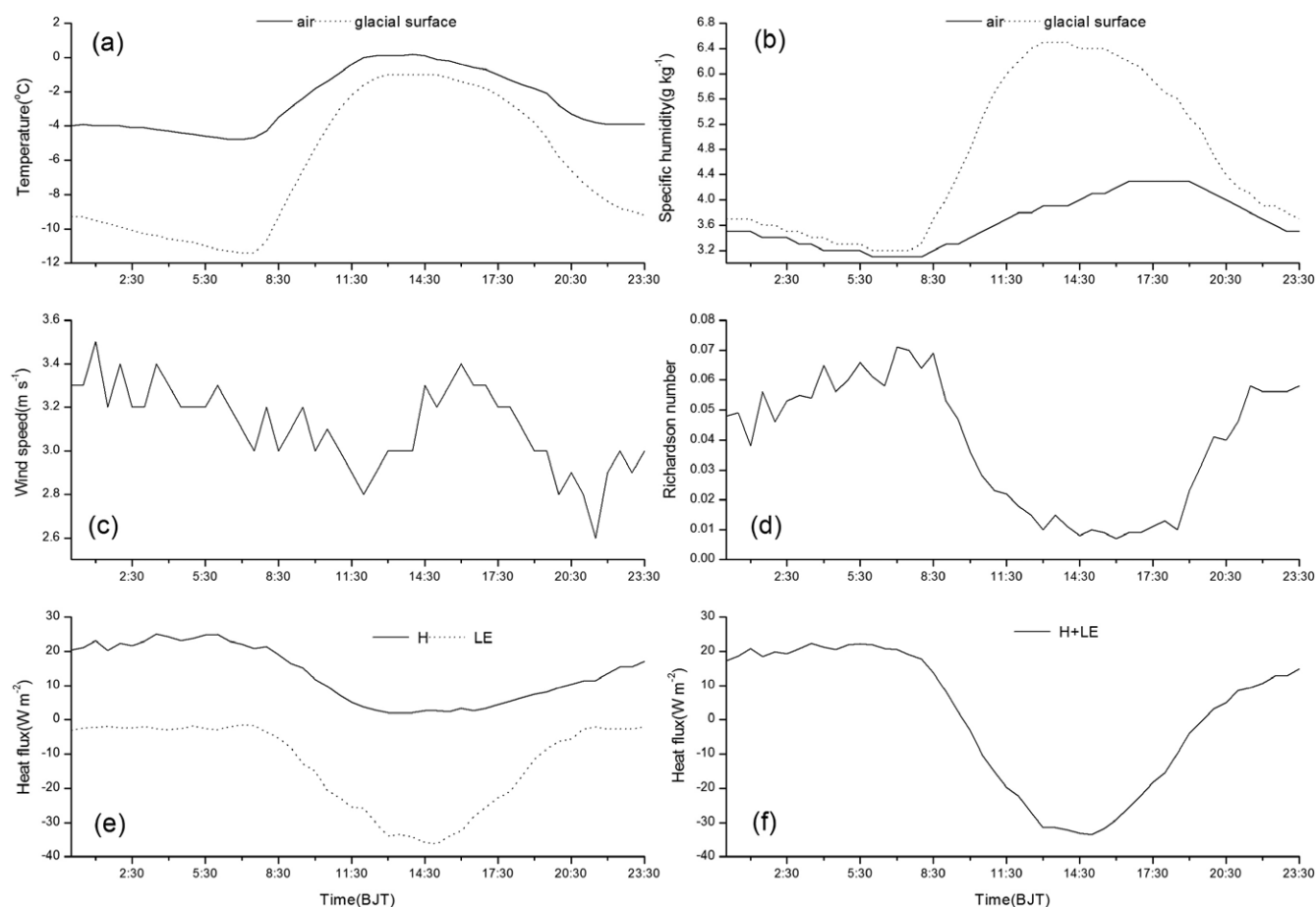

FIGURE 6. Mean diurnal cycles of (a) air and glacial surface temperature, (b) air and glacial surface specific humidity, (c) wind speed, (d) Richardson number, (e) sensible (*H*) and latent (*LE*) heat fluxes, and (f) the sum of *H* + *LE* on the Laohugou Glacier No. 12 in the Qilian Mountains from 1 June to 30 September 2009.

WEIJUN SUN ET AL. / 301

glacial surface to the atmosphere. Mean values of *LE* varied between -43 and 3.5 W m^{-2}, and were positive from 5 to 7 July, and on 15 July, which indicated that condensation had occurred. *H* and *LE* were also very sensitive to wind speed and both remained high on windy days, for example on 20 and 21 September. Clear days with high air temperature, low specific humidity, and high wind speeds were advantageous for *H* to heat the glacial surface, and for strong sublimation. Although the daily mean of the sum *H* + *LE* was small, 0.2 W m^{-2}, it varied widely around the 0 scale line (Fig. 5). *H* accounted for most of the variations of the sum *H* + *LE*, because *H* was generally larger than *LE*, therefore the sum *H* + *LE* was primarily determined by *H* ($r = 0.69$, $n = 122$).

Mean diurnal cycles of temperature, specific humidity, wind speed, Richardson number, and turbulent fluxes are presented in Figure 6. The thermal gradient between air and glacial surface temperature was generally positive, and was less during the day than at night because of the influence of solar radiation (Fig. 6, part a). The difference between air and glacial surface specific humidity reached a maximum in the afternoon (Fig. 6, part b), because the surface temperature was close to 0 °C, and the glacial surface was melting. Wind speed had a pronounced diurnal cycle, and reached a peak in the afternoon (Fig. 6, part c). Glacial surface air flow was stable most of the time ($Ri_b \geq 0.02$), and tended to a neutral condition as the glacial surface temperature increased (Fig. 6, part d). After sunrise, the gradient between air and surface temperature decreased, and *H* became gradually weaker until it reached a minimum of 1.8 W m^{-2} at 13:30 BJT. *H* then increased while the air was slowly cooled by the colder surface, and after midnight it was relatively stable until sunrise of the following day. In contrast, the minimum for *LE*, -36.3 W m^{-2}, occurred at 15:00 BJT, which indicated that there was a maximum cooling effect and maximum sublimation at that time (Fig. 6, part e). Because *H* was positive and *LE* was negative (Fig. 6, part e), they canceled each other out, producing a pronounced diurnal cycle. During the day, the magnitude of *LE* was greater than *H*, so the sum *H* + *LE* was determined by the former, and became negative. At night, *H* was larger than *LE*, therefore the sum gradually became positive (Fig. 6, part f).

COMPARISON BETWEEN CALCULATED AND MEASURED MASS BALANCE

In the accumulation zone of the Laohugou Glacier No. 12, specific mass balance was calculated from daily snow depth in water equivalents recorded by the sonic ranging sensor (e.g., Oerlemans and Klok, 2002; Mölg and Hardy, 2004). Because density measurements were limited in time, a mean density of 310 kg m^{-3} for snow measured was used to convert measured snow depth into water equivalent thicknesses. Figure 7 shows changes in calculated and measured accumulative daily mass balance. Accumulative daily mass balance fluctuated widely and sometimes became positive under the influence of snowfall (e.g. on 23 June). The strongest ablation occurred in the period 13 to 29 July and snowmelt stopped around 12 September. Measured mass balance from the sonic ranging sensor was -72 mm w.e. from 1 June to 30 September. Calculated value from the energy balance was -75 mm w.e. for this same period, a 4% overestimation compared to the measured value. The largest discrepancy between calculated and measured values

occurred in late September when there was no snowmelt, and the high wind would be responsible for the sonic height ranger data (Fig. 2).

SURFACE ENERGY BUDGET

Based on the measured net radiation and the calculated sensible and latent heat fluxes (Table 2), the surface energy budget was estimated according to the energy balance equation. The surface energy budget in the accumulation zone of the Laohugou Glacier No. 12 had special characteristics in summer. The mean value of R_n was twice as large as that of *H* in the inputs of the surface energy budget. Therefore, R_n was the principal heat source and *H* the second. The maximum value of R_n occurred in July as a result of larger cloud cover compared to other months and the maximum of *H* occurred in August as a result of higher wind speed and greater difference between air and surface temperatures. The mean value of Q_M, which was used for melting, was as large as the sum of *LE* and Q_G in the outputs of the surface energy budget. Therefore, Q_M was the principal energy sink. The proportion of *LE* in June and August exceeded 40% because of the greater difference between air and surface specific humidity during those months.

Discussion

To understand the response of the glacial accumulation zone to climate forcing during the ablation period (1 June to 30 September) in a cold, high altitude, and arid area, the correlation between Q_M and albedo was investigated, combined with precipitation and daily positive accumulated temperature (the sum of positive air temperatures at half-hourly intervals. Albedo is one of the most important factors affecting the distribution of net shortwave radiation on the glacial surface, and it governs the variation of Q_M (Mölg and Hardy, 2004). In the accumulation zone of the Laohugou Glacier No. 12, there was a close relationship between R_n and Q_M ($r = 0.87$, $n = 122$) on a daily time scale, mainly because R_n was the principal heat source and responsible for the glacier melting. There was a less pronounced, but still appreciable, relationship between Q_M and albedo ($r = -0.48$, $n = 122$), because both net shortwave and net longwave radiation influenced R_n. Although net shortwave radiation was greater than net longwave radiation, they were of the same order. Therefore, the Q_M was controlled by both net shortwave and net longwave radiation, a phenomenon that differed from findings on the Antizana Glacier (0°28′S, 78°0.9′W) in the tropical Andes of Ecuador (Favier et al., 2004). Q_M on the Antizana Glacier was dominated by net shortwave radiation, not net longwave radiation. The primary reason was that the glacial surface albedo in the accumulation zone of the Laohugou Glacier No. 12 was greater than that in the ablation zone of the Antizana Glacier. The impact of precipitation and daily positive accumulated temperature on the melting process is shown in Figure 8. After several days with successive daily positive accumulated temperatures, but without precipitation, the curve of albedo showed a steady decline. Variations of Q_M occurred in the opposite direction. After heavy snowfalls, albedo increased sharply and Q_M weakened rapidly. However, the transformation of snow resulted in a continuous albedo decline in on the glacial surface. For instance, albedo decreased and finally dropped to 0.52 as a result of continuous large
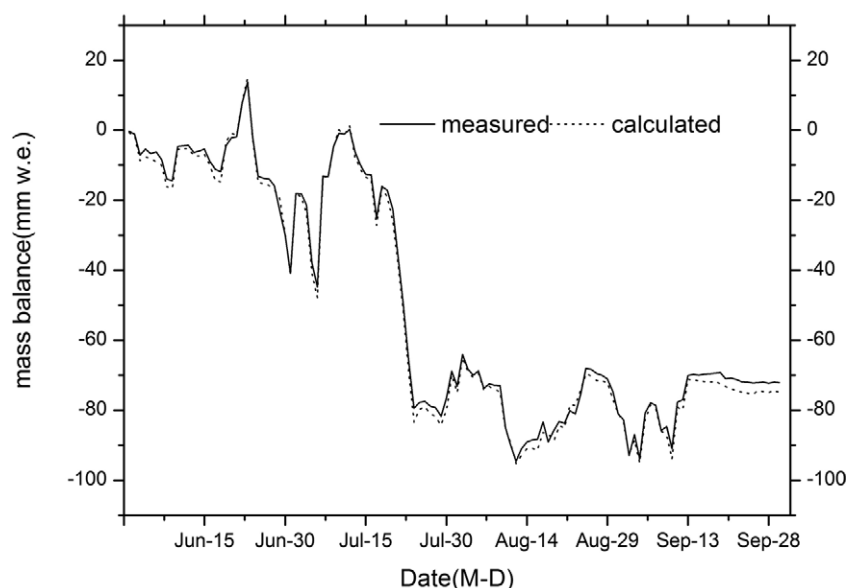
FIGURE 7. Calculated and measured accumulative daily mass balance on the Laohugou Glacier No. 12 in the Qilian Mountains from 1 June to 30 September 2009.

TABLE 2

Components of the surface energy budget at 5040 m a.s.l. on the Laohugou Glacier No. 12 in the Qilian Mountains from 1 June to 12 September 2009.

Month	Input (W m^{-2})		Output (W m^{-2})			Input (%)		Output (%)		
	R_n	H	LE	Q_G	Q_M	R_n	H	LE	Q_G	Q_M
Jun.	29.6	11.4	−18.6	−10	−12.4	72	28	45	24	31
Jul.	38.9	8.7	−8.7	−7.6	−31.3	82	18	18	16	66
Aug.	19.9	13.2	−14.4	−7.6	−11.1	60	40	44	23	33
Sep. [a]	21.0	7.6	−5.7	−5.2	−17.7	73	27	20	18	62
Mean	27.3	10.3	−11.9	−7.6	−18.2	72	28	32	20	48

[a]Mean values of Sep. are calculated from 1 to 12 September.
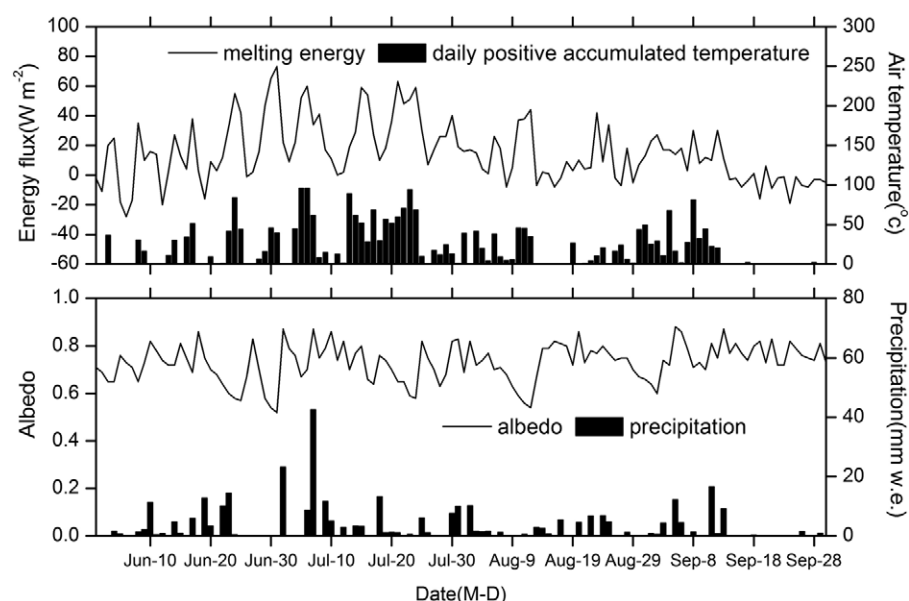

FIGURE 8. Daily positive accumulated temperature, daily mean values of albedo, and melting energy and precipitation on the Laohugou Glacier No. 12 in the Qilian Mountains from 1 June to 30 September 2009.

WEIJUN SUN ET AL. / 303

accumulated positive temperatures from 28 June to 1 July, but it rose to 0.87 after a snowfall, and glacier melting also decreased noticeably (Fig. 8). Over the next few days, without precipitation, albedo fell to 0.67, and as a result, Q_M climbed to 60 W m^{-2} on 5 July. Albedo and Q_M were therefore affected conversely by precipitation and the daily positive accumulated temperature. When the influence of precipitation was weaker than that of the daily positive accumulated temperature, a lower albedo and stronger melting were observed, as seen on 15 July. In contrast, when the influence of precipitation was stronger, a higher albedo and weaker melting were observed as seen on 5 September.

H and LE have a close relationship with the main uncertainty in the surface energy balance (Brock et al., 2010). Although the bulk aerodynamic approach can be applied to the glacial surface, much uncertainty still exists in the computation of turbulent fluxes. In order to estimate the uncertainty in the calculation of H and LE under the influence of climate variables, Table 3 illustrates the sensitivity of sensible and latent heat fluxes to uncertainty in parameter values and meteorological variables. The size of roughness lengths was concerned in discussion. Most theoretical work has demonstrated that z_{om} is 1 or 2 orders of magnitude higher than z_{ot} and z_{oq} (e.g., Andreas, 1987; Morris, 1989; Hock and Holmgren, 1996). When assuming $z_{om} = z_{ot} = z_{oq}$, H and LE were sensitive to uncertainties in the roughness lengths, while the influence of the hypothesis of $z_{om} \neq z_{ot} = z_{oq}$ on LE was minimal. The main reason was z_{om} was three times as large as z_{ot} or z_{oq}, and the value of z_{ot} was close to z_{oq}. Therefore, the selection of roughness lengths for calculating the turbulent fluxes should be treated with caution. With the assumption of neutral atmospheric conditions, the turbulent fluxes, especially H, were overestimated. It was therefore necessary to implement a stability correction to calculate the turbulent fluxes accurately. To evaluate the effect of measured sensor error on turbulent fluxes, accuracy changes in the meteorological input variables air and surface temperature, air specific humidity, and wind speed are shown in Table 3. Positive changes in these variables lead to no more than 10% increase of turbulent fluxes. Compared to effect of the first three variables on the turbulent fluxes, H and LE were less sensitive to the latter four meteorological variables. If the accuracy of the turbulence fluxes was assumed to be $\pm 10\%$, the resultant error in melting energy (27.3 W m^{-2}; Table 2) was only ± 0.2 W m^{-2}, which was minimal, because H and LE canceled each other out.

The daily variability of the surface energy budget is large, mainly as a result of variability in cloud cover and wind speed.

Cloud cover influences net radiation, and wind speed influences turbulent fluxes (Wagnon et al., 2003). The comparison of the surface energy budget was compared among extremely dry (1 July) and extremely wet conditions (2 July with precipitation of 17 mm). On 1 July, R_n (92 W m^{-2}) was 4 times greater than on 2 July, and Q_M (-73 W m^{-2}) was 3.5 times as large as on 2 July. There were many turbulent exchanges (H of 9 W m^{-2} and LE of -16 W m^{-2}) at the glacial surface on 1 July, while few turbulent exchanges (H of 2 W m^{-2} and LE of -1 W m^{-2}) occurred on 2 July. Consequently, high energy exchanges occur at the glacial surface on dry days and the ablation of the Laohugou Glacier No. 12 would increase during the ablation period (1 June to 30 September). Chen et al. (2007) have previously concluded that net radiation is the most important energy source for melting (65.5 W m^{-2}/82.4%), and turbulent fluxes were 14 W m^{-2}/17.6% for H, and -10.2 W m^{-2}/12.8% for LE, at the July 1st Glacier in the Qilian Mountains. The turbulent values are similar to those observed at the Laohugou Glacier No. 12 (Table 2), but proportions of the components of the surface energy budget are different. The reason for this difference is that measurements on the July 1st Glacier were carried out in the ablation zone where there was lower albedo on the glacial surface. To test the response of the glacier to expected climate change, some input parameters were changed (1 °C warming, 25% precipitation increase, and 0.1 albedo decrease). The results varied for R_n, H, LE, and mass balance over the period 1 June to 12 September (table not shown). The sum of H and LE increased by 7.6 W m^{-2} and mass balance decreased by 126 mm w.e. with a hypothetical 1 °C warming. Mass balance increased by 79 mm w.e., when a 25% increase in precipitation was used as input for calculation. If albedo was reduced by 0.1, R_n would increase by 26 W m^{-2} and mass balance would decrease by 489 mm w.e.

Conclusions

To better understand the glacial response to climate change, and the melting processes on the accumulation zone of the Laohugou Glacier No. 12, the essential characteristics of surface energy budget were investigated on a cold, high altitude continental glacier in an arid area, from 1 June to 30 September 2009. Net radiation was the primary source of surface energy, accounting for 72%, followed by the sensible heat flux. Q_M was the main output of the surface energy budget, and was nearly as large as the sum of LE (32%) and Q_G (20%). The modeled mass balance was -75 mm w.e., and it compared well with the values measured from sonic ranging sensor readings. A high albedo slowed down the melting on the glacial surface in the accumulation zone as a result of the snow underlying the surface. Continuous precipitation led to a reduction in melting, and melting ceased when the daily accumulated positive temperature did not reach positive values during the day. The turbulent fluxes were overestimated, especially H (by 54%), under the assumption of neutral atmospheric conditions. Therefore a stability correction was necessary, and proved to be an effective solution to the accurate calculation of the turbulent fluxes.

There have been few meteorological studies of surface energy budget on mountain glaciers in China and such measurements still need to be conducted at other sites. The energy balance model accurately describes the physical processes of melting at the glacial surface, but there are some uncertainties in the calculation of turbu-

TABLE 3

Sensitivity of the sensible and latent heat fluxes to uncertainty in parameter values and meteorological variables.

Parameter/Variable	$H(\%)$	$LE(\%)$
$z_{om} = z_{ot} = z_{oq}$	+17%	+13%
$z_{om} \neq z_{ot} = z_{oq}$	—	−2%
Neutral stability	+54%	+13%
$T \pm 0.2$ °C	±6%	±6%
$T_s \pm 0.2$ °C	±6%	±6%
$q \pm 3\%$	—	±9%
$u \pm 0.3$m s^{-1}	±10%	±9%

lent fluxes. Therefore, a detailed eddy covariance investigation of turbulent fluxes would be particularly helpful.

Acknowledgments

References Cited

Andreas, E. L., 1987: A theory for scalar roughness and the scalar transfer coefficient over snow and sea ice. *Boundary Layer Meteorology*, 38: 159–184.

Arck, M., and Scherer, D., 2002: Problems in the determination of sensible heat flux over snow. *Geografiska Annaler*, 84A(3/4): 157–169.

Bintanja, R., and Van den Broeke, M., 1995: The surface energy balance of Antarctic snow and blue ice. *Journal of Applied Meteorology*, 34: 902–926.

Bolton, D., 1980: The computation of equivalent potential temperature. *Monthly Weather Review*, 108: 1046–1953. [please check the page numbers]

Brock, B. W., Mihalcea, C., Kirkbride, M. P., Diolaiuti, G., Cutler, M. E. J., and Smiraglia, C., 2010: Meteorology and surface energy fluxes in the 2005–2007 ablation seasons at the Miage debris-covered glacier, Mont Blanc Massif, Italian Alps. *Journal of Geophysical Research*, 115: D09106, http://dx.doi.org/10.1029/2009JD013224.

Brugman, M. M., 1991: Scale dependent albedo variations and runoff from a glacierized alpine basin. *Snow, Hydrology and Forests in High Alpine Areas*, IAHS Publ., 205: 61–71. [what is the name of the editor of this volume?]

Chen, L., Duan, K. Q., Wang, N. L., Jiang, X., He, J. Q., Song, G. J., Xie, J., 2007: Characteristics of the surface energy balance of the Qiyi glacier in Qilian Mountains in melting season. *Journal of Glaciology and Geocryology*, 29(6): 882–888 (in Chinese).

Denby, B., and Snellen, H., 2002: A comparison of surface renewal theory with the observed roughness length for temperature on a melting glacier surface. *Boundary-Layer Meteorology*, 103(3), 459–468.

Du, W. T., Qin, X., Liu, Y. S., and Wang, X. F., 2008: Variation of the Laohugou Glacier No. 12 in the Qilian Mountains. *Journal of Glaciology and Geocryology*, 30(3): 373–379 (in Chinese).

Favier, V., Wagnon, P., Chazarin, J. P., Maisincho, L., and Coudrain, A., 2004: One-year measurements of surface heat budget on the ablation zone of Antizana Glacier 15, Ecuadorian Andes. *Journal of Geophysical Research*, 109: D18105, http://dx.doi.org/10.1029/2003JD004359.

Greuell, W., and Smeets, P., 2001: Variations with elevation in the surface energy on the Pasterze (Austria). *Journal of Geophysical Research*, 106(D23): 31717–31727.

Hock, R., and Holmgren, B., 1996: Some aspects of energy balance and ablation of Storglaciären, Sweden. *Geografiska Annaler*, 78A: 121–31.

Hoffman, M. J., Fountain, A. G., and Liston, G. E., 2008: Surface energy balance and melt thresholds over 11 years at Taylor Glacier, Antarctica. *Journal of Geophysical Research*, 113: F04014, http://dx/doi.org/10.1029/2008JF001029.

Jiang, X., 2008: *Observation and Modeling of the Surface Energy and Mass Balance of July 1st Glacier at Qilian Mountains in China during the Summer Ablation Period*. Lanzhou: Cold and Arid Regions Environmental and Engineering Research Institute, Chinese Academy of Sciences (in Chinese).

Kang, E. S., and Ohmura, A., 1994: A parameterized energy balance model of glacier melting on the Tianshan Mountains. *Acta Geographica Sinica*, 49(5): 467–476 (in Chinese).

Klok, E. J., Nolan, M., and Broeke, M. R. V. D., 2005: Analysis of meteorological data and the surface energy balance of McCall Glacier, Alaska, USA. *Journal of Glaciology*, 51(174): 451–461.

Li, J., Liu, S. Y., and Zhang, Y., 2007: Snow surface energy balance over the ablation period on the Keqicar Baxi Glacier in the Tianshan Mountains. *Journal of Glaciology and Geocryology*, 29(3): 366–373 (in Chinese).

Liu, Y. S., Qin, X., Du, W. T., Sun, W. J., and Hou, D. J., 2010: Analysis of the movement features of the Laohugou Glacier No. 12 in the Qilian Mountains. *Journal of Glaciology and Geocryology*, 32(3): 475–479 (in Chinese).

Mölg, T., and Hardy, D. R., 2004: Ablation and associated energy balance of a horizontal glacier surface on Kilimanjaro. *Journal of Geophysical Research*, 109: D16104, http://dx.doi.org/10.1029/2003JD004338.

Morris, E. M., 1989: Turbulent transfer over snow and ice. *Journal of Hydrology*, 105: 205–223.

Oerlemans, J., 1991: The mass balance of the Greenland ice sheet: sensitivity to climate change as revealed by energy-balance modeling. *Holocene*, 1(1): 40–49.

Oerlemans, J., and Klok, E. J., 2002: Energy balance of a glacier surface: analysis of automatic weather station data from the Morteratschgletscher, Switzerland. *Arctic, Antarctic, and Alpine Research*, 34(4):477–485.

Oke, T. R., 1987: *Boundary Layer Climates*. 2nd edition. New York: Routledge, 435 pp.

Roode, S. R., Bosveld, F. C., and Kroon, P. S., 2010: Dew formation, eddy-correlation latent heat fluxes, and the surface energy imbalance at Cabauw during stable conditions. *Boundary Layer Meteorology*, 135: 369–383.

Shi, Y. F., 1988: *An Introduction to the Glaciers in China*. Beijing: Science Press (in Chinese).

Van As, D., 2011: Warming, glacier melt and surface energy budget from weather station observations in the Melville Bay region of northwest Greenland. *Journal of Glaciology*, 57(202): 208–220.

Van den Broeke, M., Reijmer, C., and Wal, R. V. D., 2004a: Surface radiation balance in Antarctica as measured with automatic weather stations. *Journal of Geophysical Research*, 109: D09103, http://dx.doi.org/10.1029/2003JD004394.

Van den Broeke, M., As, D. V., Reijmer, C. and Wal, R. S. V. D., 2004b: Assessing and improving the quality of unmanned radiation observations in Antarctica. *Journal of Atmospheric and Oceanic Technology*, 21:1417–1431.

Wagnon, P., Sicart, J. E., Berthier, E., and Chazarin, J. P., 2003: Wintertime high-altitude surface energy balance of a Bolivian glacier, Illimani, 6340 m above sea level. *Journal of Geophysical Research*, 108(D6): 4177, http://dx.doi.org/10.1029/2002JD002088.

Wang, Z. T., 1981: *Glacier Inventory of China I: Qilian Mountains*. Lanzhou: Lanzhou Institute of Glaciology and Cryopedology (in Chinese).

Yang, X. G., Qin, D. H., Zhang, T. J., Kang, S. C., Qin, X., and Liu, H. Y., 2010: Seasonal characteristics of surface radiative fluxes on the East Rongbuk Glacier in the slope of Mt. Qomolangma (Mt. Everest) region. *Acta Meteorologica Sinica*, 68(1): 19–31(in Chinese).

Yao, J. M., 2009: *The Surface Energy and Water Budget in Tanggula Permafrost Region on the Tibetan Plateau*. Lanzhou: Cold and Arid Regions Environmental and Engineering Research Institute, Chinese Academy of Sciences (in Chinese).

Zhang, Y. S., Yao, T. D., Pu, J. C., Ohata, T., Yabuki, H. and Fujita, K., 1996: Energy budget at ELA on Dongkemadi Glacier in the Tonggula Mts. Tibetan Plateau. *Journal of Glaciology and Geocryology*, 18(1): 10–19 (in Chinese).

MS accepted March 2012